ACS Catalysis

Letter

pubs.acs.org/acscatalysis

Migration of Cu Ions in SAPO-34 and Its Impact on Selective Catalytic Reduction of NO_x with NH_3

Peter N. R. Vennestrøm,*[,†,‡] Anna Katerinopoulou,[†] Ramchandra R. Tiruvalam,[†] Arkady Kustov,[†] Poul G. Moses,[†] Patricia Concepcion,[‡] and Avelino Corma*[,‡]

[†]Research & Development Division, Haldor Topsøe A/S, Nymøllevej 55, 2800 Kongens Lyngby, Denmark

[‡]Instituto de Tecnología Química (UPV-CSIC), Consejo Superior de Investigaciones Científicas, Universidad Politécnica de Valencia, Avenida de los Naranjos s/n, 46022 Valencia, Spain

Supporting Information

ABSTRACT: Migration of copper species from the surface region upon activation of Cu−SAPO-34 leads to a several-fold increase in catalytic activity for the selective catalytic reduction of NO_x with NH_3. The temperatures required for the activation are higher than normal calcination temperatures and lead to a homogeneous transition metal distribution that renders Cu−SAPO-34 an industrially promising candidate for NO_x removal.

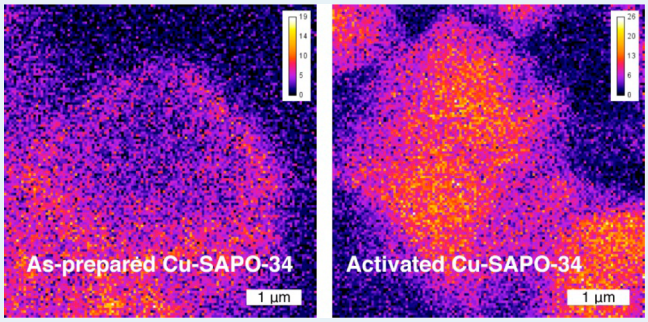

KEYWORDS: *electron microscopy, heterogeneous catalysis, nitrogen oxides, selective catalytic reduction, zeolites*

NO_x and particulate matter from internal combustion diesel engines are among the largest air pollution contributors, and therefore, legislative demands are becoming increasingly stringent. For diesel automotive exhaust treatment systems, one of the most promising practical solutions to remove NO_x and soot particles is the use of selective catalytic reduction of NO_x with NH_3 (NH_3-SCR) and a catalytic diesel particulate filter (DPF). Integration of SCR and DPF functionality is furthermore often required because of spacial limitations. Active regeneration of the DPF requires catalyst hydrothermal stability above 750 °C, which can be obtained using small-pore copper-exchanged zeolites, since the presence of 8-member ring windows in the microporous structure is known to limit catalyst degradation.[1]

Zeolithic materials with CHA topology (see e.g. ref 2), are already applied and among the most promising candidates for combined NH_3-SCR/DPF. The CHA topology consists of a three-dimensional porous system with cavities and small-pore, 8-member ring windows with a free diameter of 3.8 × 3.8 Å.[3] The high silica zeolite with CHA topology is usually referred to as SSZ-13[4] (T-atoms = Si + Al) and its silicoaluminophosphate (T-atoms = Si + Al + P) analog as SAPO-34. Ironically, the presence of small-pore windows in combination with the hydrophilic nature of silicoaluminophosphates[5] makes the introduction of catalytically active copper sites more difficult in SAPO-34, especially by aqueous exchange. Other methods could include gas-phase exchange with CuCl[6] or solid-state exchange with CuO.[7] Herein, we reveal that during aqueous ion exchange, the introduction of Cu into SAPO-34 occurs only in the outer parts of the crystals. This renders a catalytically inactive material, but upon activation at high temperature, copper species migrate from the surface region into the crystals, giving an almost homogeneous distribution. After activation, a several-fold increase in catalytic activity is experienced, yielding Cu−SAPO-34 as an industrially relevant catalyst for the NH_3-SCR reaction. This opens up for the use of hydrothermally stable and highly active Cu−SAPO-34 as an alternative to Cu−SSZ-13 and other transition-metal-exchanged zeolites in automotive applications. Furthermore, because activation of metal-exchanged SAPO materials has earlier been overlooked, their catalytic potential may have been underestimated.

Choosing the right crystal size of SAPO-34 for the NH_3-SCR reaction is based on a trade-off. Large crystals are in general more (hydro)thermally stable than small ones because of the larger periodicity; however, diffusion limitations in CHA materials, as recently described for NH_3-SCR,[8] become increasingly more severe when the crystal size is increased (see Supporting Information for a comparison of crystal sizes). In addition, in the current study, we present that ion exchange of SAPO materials, in particular, small-pore versions, is nontrivial. Table 1 summarizes the effect crystal size has on the maximum possible amount of Cu that can be introduced into the material for a given Cu concentration in the solution. Under similar ion exchange conditions, the obtained copper content decreases monotonically when the average crystal size

Received: July 3, 2013
Revised: August 7, 2013
Published: August 8, 2013

Table 1. Average Crystal Sizes, Si Content and NH_3 Capacity of SAPO-34 Materials as well as Atomic Ratios of Cu to Tetrahedrally Coordinated Framework Atoms (T-atoms = Si, Al, P) after Aqueous Exchange with 5 mM or 125 mM Cu^{2+} Concentrations

Φ[a] (μm)	Si/ T-atom[b]	NH_3 cap.[c] (μmol/g)	IE 5 mM[d] Cu/(T-atom)	IE 125 mM[d] Cu/(T-atom)
1.0	0.10	915	7.88×10^{-3}	14.69×10^{-3}
3.7	0.14	985	5.00×10^{-3}	11.59×10^{-3}
6.2	0.11	960	3.86×10^{-3}	8.44×10^{-3}
11	0.10	1038	2.67×10^{-3}	7.65×10^{-3}

[a]Average crystal size (determined by SEM and electroacoustic methods). [b]Elemental silicon content (Si/(Si + Al + P). [c]NH_3 capacity measured after saturation and purging at 150 °C, followed by desorption up to 600 °C. [d]IE = ion exchange with the given concentration of $Cu(OAc)_2$ for 24 h with 250 mL/g

increases (see Table 1) and is not directly related neither to the Si content nor to the number of acid sites measured here by NH_3-TPD.

An increase in the ion exchange time did not yield a corresponding increase in copper content. For crystallites with an average size of 3.7 μm, the obtained copper content increased from 11.6×10^{-3} only to 13.7×10^{-3} Cu atoms per tetrahedral framework atom (Si + Al + P) when the time was increased from 24 to 120 h. The latter corresponds to 1.2 wt % of Cu in the final Cu−SAPO-34, and this material was chosen as the model material for further studies. Furthermore, it was also observed that an increase in the exchange concentration above 125 mM or changing the copper salt used did not lead to a significant increase in the copper content.

Higher copper contents obtained for smaller crystals suggest that the copper is not homogeneously distributed (as also recently pointed out by Wang et al.[9]) but, instead, is related to the external surface. We therefore decided to test the possibility of redistributing it thermally by systematically heating the as-prepared Cu−SAPO-34 between 250 and 850 °C. To monitor the impact of redistributing the Cu, changes in catalytic activity were measured in the low temperature regime at 180 °C to minimize contributions from diffusion limitations and because this is the lowest temperature at which urea can be dosed in practical applications. Catalytic TOF for the NH_3-SCR reaction increased more than 5-fold upon this treatment, as can be seen in Figure 1.

In comparison, the aluminosilicate zeolite Cu−SSZ-13 was almost unaffected by the thermal treatment up to 850 °C. In contrast, Cu−SAPO-34 initially showed poor activity, but increases to a similar or slightly higher activity as Cu−SSZ-13, independent of copper load, under typical calcination temperatures of 550 °C and up to almost double that of Cu−SSZ-13 at higher temperatures.

Turnover frequencies (TOFs) were calculated on the basis of obtained pseudo-first-order rate constants, assuming that the reactions follow a first-order dependence in NO and zero in NH_3.[10] We furthermore confirmed that the increase in activity is proportional to the Cu load for Cu−SAPO-34 in the range of Cu used (see Supporting Information).

After heating to 750 °C, the activation energy for the NH_3-SCR reaction over Cu−SAPO-34 became 69.1 kJ/mol. In comparison, Cu−SSZ-13 showed an activation energy of 69.3 kJ/mol, irrespective of the activation. However, when Cu−SAPO-34 was not activated at higher temperatures, the activation energy was only 38.6 kJ/mol (see Supporting Information). The activation energy for diffusion is smaller than for chemical reactions, and therefore, an increase in the apparent activation energy indicates removal of a diffusion barrier (others have reported even lower E_a barriers over ion-exchanged SAPO-34[11]).

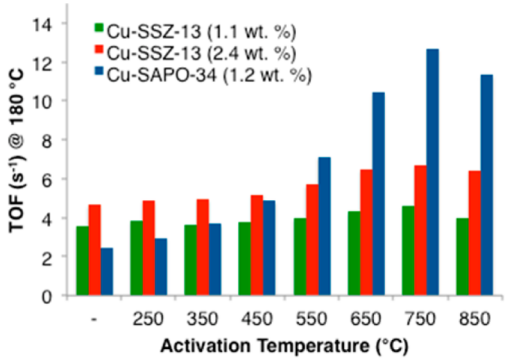

Figure 1. Catalytic TOF ($mol_{gas}/mol_{Cu}/s$) of Cu−SAPO-34 (1.2 wt %) and Cu−SSZ-13 (1.1 and 2.4 wt %), depending on activation treatment. Catalytic test conditions were the following: 500 ppm NO, 530 ppm NH_3, 10% O_2, 5% H_2O, balance N_2 to a total flow of 300 NmL/min and 10 mg catalyst. Activations were performed at the indicated temperature for 1 h in a flow of 10% O_2 and 90% N_2.

The loss of accessibility for small molecules after ion exchange can also be perceived by nitrogen physisorption measurements of the micropore volume. In the parent SAPO-34, 0.21 cm^3/g is accessible, whereas only 0.16 cm^3/g is available after ion exchange. After an activation at 750 °C, most of the micropore volume could be recovered and reach 0.20 cm^3/g. This shows that exchange and activation does not lead to a collapse of the crystal structure, as was also confirmed by XRD (see Supporting Information), but that Cu blocks the micropore system before activation, despite the three-dimensional pore system.

To explain the increase in catalytic performance shown in Figure 1, X-ray photoelectron spectra (XPS) were recorded after increasing high-temperature treatments (250−750 °C) on Cu−SAPO-34 and on Cu−SSZ-13. XPS using an Al Kα X-ray source gives an average sampling depth of 4.5 nm for Cu 2p and for microporous materials such as the CHA structure. This is slightly increased as a result of the large void fraction in zeolithic materials.[12] Thus, more than 2−3 hexagonal unit cells with 36 T-atoms are probed in this way.

It is clear from Figure 2 that upon heating Cu−SAPO-34 Cu migrates from the surface and the outer unit cells into the material, as witnessed by the decrease in the Cu $2p_{3/2}$ peak. In comparison, no changes in the surface concentration of Cu in Cu−SSZ-13 before and after activation at 750 °C could be observed.

The Cu $2p_{3/2}$ binding energies (BE) observed in the XPS spectra measured on as-prepared Cu−SSZ-13 and Cu−SAPO-34 are initially similar and located at 933.3 eV. Although the two samples have similar BEs, Cu−SAPO-34 also has a small contribution in the Cu L_3VV Auger spectra at kinetic energies (KE) of ca. 917 eV (Supporting Information), which has earlier been ascribed to copper oxide at the surface of zeolites,[13] but this is consumed after activation above 250 °C. For all other treatments and irrespective of material, the Cu L_3VV Auger peaks are observed only below 915 eV, which is consistent with copper being located in ion-exchange positions. After heating to 250 °C, the largest contribution to the Cu $2p_{3/2}$ BE in Cu−

dx.doi.org/10.1021/cs400499p | ACS Catal. 2013, 3, 2158−2161

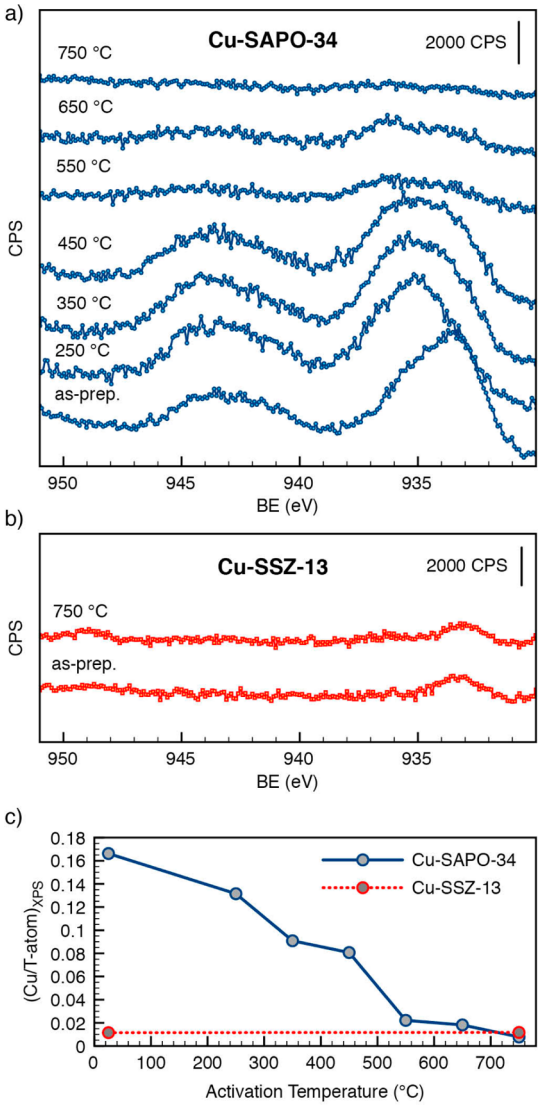

Figure 2. X-ray photoelectron spectra of the Cu $2p_{3/2}$ region of (a) Cu−SAPO-34 (1.2 wt %), (b) Cu−SSZ-13 (2.4 wt %) before and after activation at various temperatures given in the figure for 1 h, and (c) quantification of the Cu/T-atom ratio in the surface from XPS. Activations were performed ex situ in a flow of dry technical air.

SAPO-34 is shifted to higher energies (935.6 eV), and further heating causes peak broadening due to the presence of at least two states of Cu, most likely corresponding to the heterogeneity of exchange environments, such as isolated Si sites (Q^1 sites) or edges of Si islands (Q^2 and Q^3 sites), as often observed by ^{29}Si-MAS NMR, inside SAPO materials with high Si contents, where the remaining copper species are located. In comparison, the Cu $2p_{3/2}$ photo electron BE remains unaffected in Cu−SSZ-13 after heating to 750 °C, indicating that no overall migration has taken place in this system after the heat treatment.

Furthermore, the migration of copper species in Cu−SAPO-34 occurs in at least two discrete steps: one at low temperatures (250−450 °C) and one at higher temperatures (450−750 °C). Quantification of the Cu/T-atom ratio in the surface from the XPS spectra (see bottom panel in Figure 2), where two slopes are seen in the two temperature regimes, further confirms this observation but also indicates that only after 750 °C activation is the copper not predominantly located at the surface (compare Cu/T-atom ratio for Cu−SSZ-13 and Cu−SAPO-34).

We note that at the high Si concentration (Si/(T-atom) = 0.14) in the present materials, one finds that two different coordination sequences would dominate, with either one Al between Si atoms or a sequence of two Al and one P atom. This coincides with the existence of two characteristic migration temperatures, and we propose that the two characteristic migration temperatures could result from a dependence of the diffusion rate of Cu species on the Si coordination sequences in the SAPO-34 material.

The XPS results alone are not sufficient to describe how the copper distributes upon the activation, and several scenarios may be envisioned. To further visualize the copper migration, the distribution of Cu was recorded by characteristic X-ray intensity maps in Cu−SAPO-34 (see Figure 3) before and after activation at 750 °C (Si, Al, and P maps are given in the Supporting Information). Maps were recorded on more than 10 crystals randomly chosen. Beam damage due to material instability under the beam could be minimized using low dwell times and averaging over several accumulations. Beam tracking was also applied to avoid lateral drift, which would otherwise have affected the spatial resolution. In all cases, a copper rim was visible in the surface of the Cu−SAPO-34 in the as-

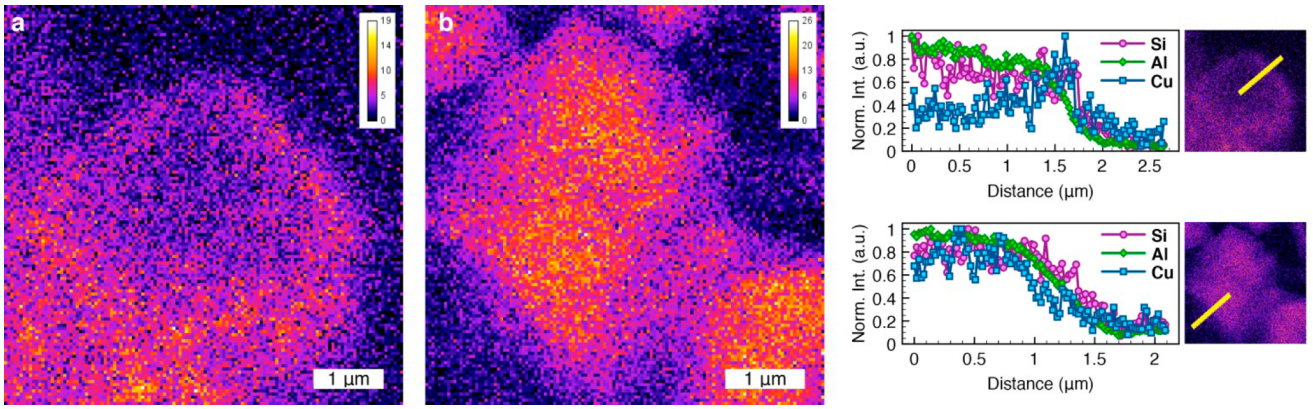

Figure 3. (Left) Pseudocolor representation of the spacial difference in Kα X-ray intensity for Cu in (a) as-prepared Cu−SAPO-34 and (b) Cu-SAPO-34 after activation at 750 °C Cu−SAPO-34. (Right) comparison of normalized X-ray intensities for Si (purple), Al (green), and Cu (blue) in as-prepared Cu-SAPO-34 (top) and after activation (bottom). Data were extracted from the maps at the areas indicated by the yellow lines and averaged over 10 pixels, corresponding to the line thickness.

dx.doi.org/10.1021/cs400499p | ACS Catal. 2013, 3, 2158−2161

prepared sample, and a homogenous distribution of Cu in the activated sample was observed. The copper rim in as-prepared Cu−SAPO-34 (Figure 3a) indicates that Cu is, indeed, locally concentrated in the outer subsurface of the as-prepared SAPO-material, which is confirmed by the simultaneous increase in X-ray intensity compared with framework elements close to the surface as seen in the linescan (right panel, Figure 3). Moreover, after activation, the normalized intensity of the characteristic X-rays from framework T-atoms and Cu measured across the crystal show no individual variation in concentration across the crystal and confirm the homogeneous distribution.

Furthermore, through sample preparation, crystals that were cut in different depths and maps on the activated sample show a homogeneous Cu distribution independent of the cutting direction or depth.

In summary, we have found that copper does not readily ion exchange into the pores of SAPO-34 and that only upon a high-temperature treatment will the copper redistribute to yield an active catalyst. We find that activation leads to a homogeneous Cu distribution in Cu−SAPO-34, whereby the activity of the material in the NH_3-SCR reaction increases several-fold and becomes more active than the conventional Cu−SSZ-13 per Cu atom. This makes Cu−SAPO-34 a relevant catalyst for industrial applications. Moreover, the catalytic potential of metal-exchanged SAPO materials seems to rely on activation and could for this reason have been underestimated in the past and their catalytic potential perhaps not fully explored.

■ ASSOCIATED CONTENT

Supporting Information

Experimental details, additional characterization and further catalytic data. This material is available free of charge via the Internet at http://pubs.acs.org.

■ AUTHOR INFORMATION

Corresponding Author

*E-mail: pnrv@topsoe.dk (P.N.R.V), acorma@itq.upv.es (A.C.).

Notes

The authors declare no competing financial interest.

■ ACKNOWLEDGMENTS

This work was supported by the Danish Ministry of Science, Innovation and Higher Education and is dedicated to the legacy of Dr. Haldor Topsøe and his 100 years of dedication to catalysis and fundamental science. We furthermore thank Stig Helveg and Charlotte C. Appel for fruitful discussions and facilitation of microscopy investigations.

■ REFERENCES

(1) (a) Fickel, D. W.; D'Addio, E.; Lauterbach, J. a.; Lobo, R. F. *Appl. Catal., B* **2011**, *102*, 441. (b) Kwak, J. H.; Tran, D.; Burton, S. D.; Szanyi, J.; Lee, J. H.; Peden, C. H. F. *J. Catal.* **2012**, *287*, 203. (c) Kwak, J. H.; Tonkyn, R. G.; Kim, D. H.; Szanyi, J.; Peden, C. H. F. *J. Catal.* **2010**, *275*, 187.

(2) (a) Bull, I.; Boorse, S. B.; Jaglowski, W. M.; Koermer, G. S.; Moini, A.; Patchett, J. A.; Xue, W.-M.; Burk, P.; Dettling, J. C.; Caudle, M. T. U.S. Patent 7,601,662, 2008. (b) Gekas, I.; Johansen, K. U.S. Patent Appl. 2011/0283680 A1, 2011. (c) Anderson, P. J.; Chen, H.-Y.; Fedeyko, M.; Weigert, E. U.S. Patent 7,998,443, 2011. (d) Li, H.-X.; Cormier, W. E.; Moden, B. U.S. Patent 7,883,678, 2011.

(3) Baerlocher, C.; McCusker, L. B. Database of Zeolite Structures: http://www.iza-structure.org/databases/ (accessed August 2013).

(4) Zones, S. I. U.S. Patent 4,544,538, 1985

(5) Flanigen, E. M.; Broach, R. W.; Wilson, S. T. In *Zeolites in Industrial Separation and Catalysis*; Kulprathipanha, S., Ed.; Wiley-VCH: Weinheim, 2010, pp 1−26

(6) (a) Spoto, G.; Bordiga, S.; Scarano, D.; Zecchina. *Catal. Lett.* **1992**, *13*, 39. (b) Guidry, T.; Price, G.. *J. Catal.* **1999**, *27*, 16.

(7) (a) Kucherov, A. V.; Slinkin, A. A. *Zeolites* **1986**, *6*, 175. (b) Zamadics, M.; Chen, X.; Kevan, L.. *J. Phys. Chem.* **1992**, *96*, 5488. (c) Kanazirev, V.; Price, G.. *J. Mol. Catal. A: Chem* **1995**, *169*, 145.

(8) Gao, F.; Walter, E. D.; Karp, E. M.; Luo, J.; Tonkyn, R. G.; Kwak, J. H.; Szanyi, J.; Peden, C. H. F. *J. Catal.* **2013**, *300*, 20.

(9) Wang, L.; Gaudet, J. R.; Li, W.; Weng, D. *J. Catal.* **2013**, *306*, 68.

(10) Gao, F.; Walter, E. D.; Karp, E. M.; Luo, J.; Tonkyn, R. G.; Kwak, J. H.; Szanyi, J.; Peden, C. H.F. *J. Catal.* **2013**, *300*, 20. (b) Huang, H. Y.; Long, R. Q.; Yang, R. T. *Appl. Catal., A* **2002**, *235*, 241. (c) Delahay, R.; Kieger, S.; Tanchoux, N.; Trens, P.; Coq, B. *Appl. Catal., B* **2004**, *52*, 251. (d) Komatsu, T.; Nunokawa, M.; Moon, I. S.; Takahara, T.; Namba, S.; Yashima, T. *J. Catal.* **1994**, *148*, 427. (e) Brandenberger, S.; Kröcher, O.; Tissler, A.; Althoff, R. *Catal. Rev. Sci. Eng.* **2008**, *50*, 492.

(11) Wang, L.; Li, W.; Qi, G.; Weng, D. *J. Catal.* **2012**, *289*, 21.

(12) Grünert, W. *Characterization of Solid Materials and Heterogeneous Catalysts*, Wiley-VCH Verlag GmbH & Co. KGaA: Weinheim, 2012.

(13) (a) Grünert, W.; Hayes, N. W.; Joyner, R. W.; Shpiro, E. S.; Siddiqui, M. R. H.; Baeva, G. N. *J. Phys. Chem.* **1994**, *98*, 10832. (b) Liese, T.; Grünert, W. *J. Catal.* **1997**, *172*, 34.